

Reversible ultrafast soliton switching in dual-core highly nonlinear optical fibers

Nguyen Viet Hung¹, Le Xuan The Tai², Ignac Bugar^{3,4}, Mattia Longobucco^{3,5},

Ryszard Buczynski^{3,5}, Boris A. Malomed^{6,7} and Marek Trippenbach⁵

¹*Advanced Institute for Science and Technology, Hanoi University of Science and Technology, Hanoi, Vietnam.*

²*Faculty of Physics, Warsaw University of Technology, PL-00662 Warsaw, Poland.*

³*Department of Glass, Lukasiewicz Research Network Institute of Electronic Materials Technology, Wolczynska 133, 01-919 Warsaw, Poland.*

⁴*International Laser Centre, Ilkovicova 3, 841-04 Bratislava, Slovakia.*

⁵*Faculty of Physics, University of Warsaw, ul. Pasteura 5, PL-02-093 Warszawa, Poland.*

⁶*Department of Physical Electronics, School of Electrical Engineering, Faculty of Engineering, and Center for Light-Matter Interaction, Tel Aviv University, Tel Aviv 69978, Israel.*

⁷*Instituto de Alta Investigación, Universidad de Tarapacá, Casilla 7D, Arica, Chile.*

We experimentally investigate a nonlinear switching mechanism in a dual-core highly nonlinear optical fiber. We focus the input beam of femtosecond pulses on one core only, to identify transitions between inter-core oscillations, self-trapping in the cross core, and self-trapping of the pulse in the straight core. A model based in the system of coupled nonlinear Schrödinger equations provides surprisingly good agreement with the experimental findings.

OCIS Codes (320.7110) Ultrafast nonlinear optics; (200.6715) Switching; (060.5530) Pulse propagation and temporal solitons.

Realization of all-optical switching in a simple format has long been a challenge for nonlinear fiber optics. The concept of nonlinear directional couplers based on dual-core fibers was introduced theoretically in early 1980s [1–3]. Since then considerable efforts were devoted to the characterization and optimization of the device performance [4, 5]. In particular, a promising demonstration of ultrafast nonlinear switching had been reported utilizing femtosecond pulses in the normal-group-velocity-dispersion (GVD) range of the silica-fiber coupler [6]. The main limitations of ultrafast nonlinear switching in conventional nonlinear couplers are relatively high powers (~ 100 kW) required for the signal redirection, and the ensuing breakup in the temporal domain [6, 7]. Additionally, the switching performance is compromised by the intra-channel and inter-modal GVD, which strongly affects pulses of width ~ 100 fs. To avoid the degradation driven by these factors, it was proposed to exploit temporal solitons [8], taking advantage of their robustness. Numerous theoretical works [9–14] reported diverse schemes of the soliton switching.

Despite the theoretical advances, very few experimental studies have been performed for switching of temporal solitons in nonlinear couplers, with results remaining far behind the theoretical predictions. The experimental works, exploiting the soliton propagation in dual-core photonic-crystal fibers (PCFs) [15, 16], were hampered by the fission of naturally emerging higher-order solitons, resulting in output distributed chaotically between the two channels [17]. Later, an extensive numerical study for an air-glass dual-core PCF made of a highly nonlinear lead silicate glass (PBG-08), had revealed a possibility of self-trapping of higher-order solitons, following their self-compression [18]. Such an effect, which tends to keep a spectrally broadened pulse in one fiber core, was demonstrated in a multichannel fiber structure, as a basis of

the creation of “arrayed light bullets” [19]. Motivated by these concepts, a new study of self-trapping, alternating between the two fiber cores, was initiated, aiming at achieving high-contrast switching performance. It is focused on the performance of a highly-nonlinear dual-core fiber with two soft glass kernels. Strong nonlinearity is ensured by using the PBG-08 glass, while the complex air-glass PCF structure is replaced by a low-index glass [20]. The high-index contrast (0.4) between the core and cladding in this system supports very efficient switching performance, as predicted by simulations [21]. Moreover, a higher level of the dual-core symmetry was achieved in this fiber, in comparison to previously used dual-core PCFs, which is necessary for the operation of all-optical switching in dual-core fibers [23].

The pilot experiments in the optimized dual-core-fiber, using pulses of 100-fs duration, with carrier wavelength 1700 nm, have demonstrated, for first time, high-contrast (16.7 dB) switching in the soliton regime [22]. In the present paper we report essentially more advanced experimental results achieved in the C-band (at 1560 nm), using a new generation of strongly nonlinear high-index-contrast dual-core fibers. The experimental findings are supported by simulations which use a model with experimentally relevant parameters.

The model is based on the system of linearly-coupled nonlinear Schrödinger equations (NLSEs) [24–27], written for complex envelopes $\Psi_{1,2}(t, z)$ of electromagnetic waves in the cores

$$\begin{aligned} i\partial_z \Psi_1 &= -(1/2)\beta_2 \partial_t^2 \Psi_1 - \gamma |\Psi_1|^2 \Psi_1 - \kappa \Psi_2, \\ i\partial_z \Psi_2 &= -(1/2)\beta_2 \partial_t^2 \Psi_2 - \gamma |\Psi_2|^2 \Psi_2 - \kappa \Psi_1, \end{aligned} \quad (1)$$

where z and t are the propagation distance and time in physical units, with β_2 , γ , and κ representing, respectively, the GVD, Kerr nonlinearity, and inter-core coupling. By means of rescaling, $t = \sqrt{\beta_2/\kappa\tau} \equiv t_0\tau$,

$z = \zeta/\kappa$, $\Psi_{1,2} = \sqrt{\kappa/\gamma}A_{1,2}$, Eqs. (1) are cast in the normalized form, with β_2, γ , and κ set equal to 1. The model does not include effects of secondary importance, such as the Raman scattering, self-steepening, and higher-order GVD effects (cf. Ref. [22]), as simulations of the extended system demonstrate no essential differences, in terms of switching and retention in the straight channel, except for a uniform factor adjusting the experimental and theoretical energy scales, which is $E_{\text{exp}} \approx 1.25E_{\text{theor}}$, as produced by Eqs. (1), see below.

Simulations of this system were run with the input corresponding to the experiment performed in this work, *viz.*, a soliton-like pulse with independent amplitude a and inverse width η [28], coupled at $\zeta = 0$ into one (*straight*) channel:

$$A_1(0, \tau) = a \text{sech}(\eta\tau), \quad A_2(0, \tau) = 0, \quad (2)$$

the FWHM width of the pulse being $t_{\text{FWHM}} = 1.76t_0/\eta$.

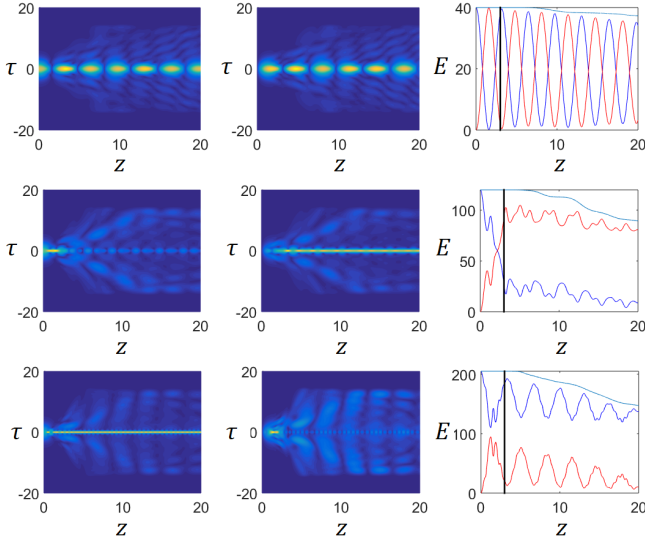


FIG. 1. The switching between channels, produced by simulations of Eq. (1) for three values of the input amplitude (2), $a = 1.15, 2.0, 2.6$ (from top to bottom), and a fixed inverse width, $\eta = 0.78$. The left and central columns display spatiotemporal patterns of the intensities, $|A_{1,2}(z, \tau)|^2$, in the straight and cross channels, respectively. The blue and red curves in the right column show the energy in each channel (and the total energy, shown by the cyan curve) vs. the propagation distance. The top, central, and bottom panels represent, severally, regimes with periodic inter-core oscillations, self-trapping in the cross channel, and retention in the straight one, respectively. The vertical line at $\zeta = 3$ denotes the length of the fiber in the experiment.

Simulations of Eqs. (1) were performed with parameters corresponding to the all-solid 4.3 cm long DCF used in the experiment. The respective parameters, produced by the Lumerical mode solver at wavelength $\lambda = 1.56 \mu\text{m}$, are the inverse group velocity $\beta_1 = 6.5610^{-9} \text{ s/m}$, $\beta_2 = -7.73 \cdot 10^{-26} \text{ s}^2/\text{m}$, $\kappa = 75 \text{ m}^{-1}$,

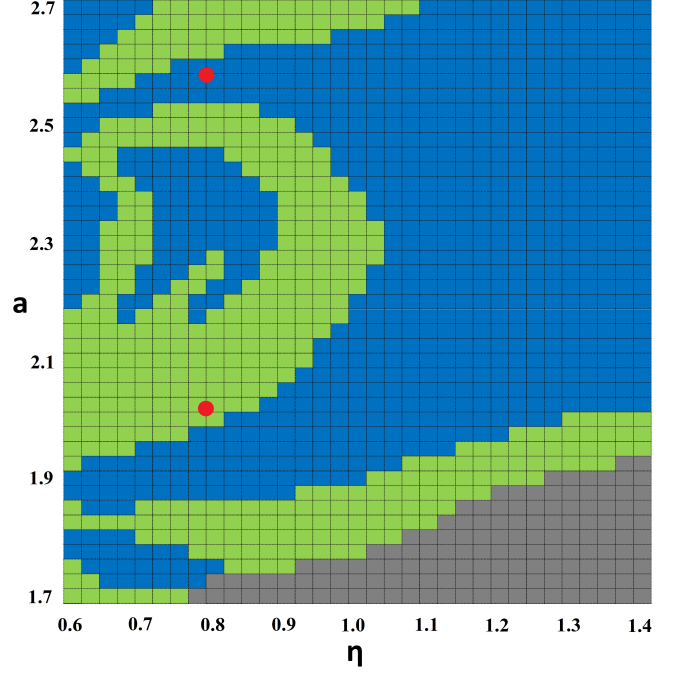


FIG. 2. The chart of dynamical regimes of the system in the (η, a) plane, produced by simulations of Eqs. (1) with input (2). Inter-core oscillations, switching into the cross channel, and trapping in the straight one occur in gray, green, and blue areas, respectively. Red circles refer to two bottom rows in Fig.1. The case shown in the top row falls in the gray area beneath the frame of the chart.

and $\gamma = 0.4 \text{ W}^{-1}\text{m}^{-1}$ (measured in [29]). Relevant units of the propagation length and time are $z_0 = 1/\kappa \approx 13 \text{ mm}$ and $t_0 \approx 32 \text{ fs}$, with $t_{\text{FWHM}} \approx 75 \text{ fs}$ and $\eta = 0.78$. In the scaled notation, the natural period of the population oscillations between the cores is π , and the length of the sample is ≈ 3 , making it appropriate for the realization of the switching. The scaled amplitude in Eq. (2), a , is related to the pulse's energy in physical units

$$E = (\kappa/\gamma) \tau_0 \int_{-\infty}^{+\infty} |A_1(0, \tau)|^2 t_0 d\tau \approx 1.14 a^2 \kappa t_{\text{FWHM}} / \gamma, \quad (3)$$

For our experimental conditions, this implies $E \approx 30a^2$ in units of pJ.

Input (2) in the single channel ($\kappa = 0$) generates intrinsic oscillations of deformed solitons (breathers). According to the exact solution of NLSE [28], the (spatial) frequency of the oscillations is $\omega = 4(a - \eta)\eta$ in interval $3/2 < a/\eta < 5/2$, in which the breather is a superposition of two fundamental solitons. As a function of η , it attains a maximum, $\omega_{\text{max}} = a$, at $\eta = a/2$.

Including coupling κ , in Fig. 1 one observes interplay between inter- and intra-channel oscillations and emission of small-amplitude waves in each channel, mostly at the initial stage of the propagation. For a smaller amplitude of the input, $a = 1.15$, *i.e.*, relatively weak nonlin-

earity, we observe quasiharmonic oscillations of the energy between the cores. At a larger amplitude, $a = 2.0$, the nonlinearity switches the quasi-soliton into the cross channel, where it gets trapped. At the largest amplitude, $a = 2.6$, strong nonlinearity keeps the energy in the straight channel, with residual oscillations of the radiation between the channels. Slow decay of the total energy, shown by cyan lines in right-hand panels, is induced by losses at absorbers, installed at edges of the time-integration domain, to emulate the radiation loss in the experiment. The losses are negligible for $\zeta \leq 3$, which corresponds to the fiber length in the experiment, 4.3 cm.

Results of simulations are summarized in Fig. 2, in a chart of three outcomes in plane (η, a) of the parameters of input (2), *viz.*, periodic oscillations (the gray area); self-trapping in the cross channel (green), and retention in the straight one (blue). The increase of a exhibits a natural trend for the transition of the oscillations into self-trapping in the cross channel, followed by the transition to the retention of strongly nonlinear pulses in the straight one. The reverse transition of the self-trapping from the straight channel to the cross one, with the further increase of a , observed in Fig. 1 at $\eta < 1$, is explained by the interplay of initial solitonic breathing and inter-core oscillations.

The experiments were performed using the above-mentioned dual-core fiber, manufactured and optimized by us which is nearly identical to the one in which the high-contrast soliton switching was demonstrated at the wavelength of 1700 nm [22]. The new fiber differs from the prototype by a larger number (six) of cladding rods in the preform, and by slower drawing speed in a different tower. The scanning electron microscope (SEM) image of the cross section structure is similar as was presented in [22], only the distance between centers of the two high-index PBG-08 glass cores increased slightly from 3.1 to 3.3 μm . The recent numerical simulation study took into consideration the real fiber parameters acquired by analysing the SEM image of the DCF cross section. Even though it is noticeable that the best experimental results were obtained at the same fiber length of 4.3 cm as predicted by the earlier numerical simulation at similar wavelength of 1500 nm, performed on totally symmetrical hexagonal core structure [20].

The experiment was run in a setup similar to one in Ref. [22]. The laser source was a Menlo C-fiber amplified oscillator, generating 3 nJ pulses at 1560 nm, with the pulse width of 75 fs, at the repetition rate of 100 MHz. The output channels of the dual-core fiber were monitored sequentially by a CCD camera (Electro Optic CamIR1550) and by an optical spectral analyzer (Yokogawa), collecting spectra separately from both. Images and spectra were recorded at each level of the input-pulse's energy. Figure 3 presents a sequence of camera images recorded with increasing input energy. These results are similar to the switching performance reported for the 1700 nm carrier wavelength

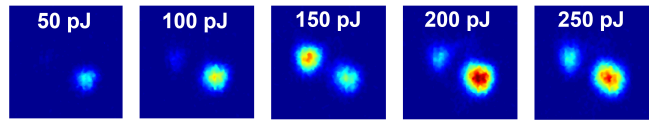


FIG. 3. A sequence of camera images of the output fiber facet for different energies of the input.

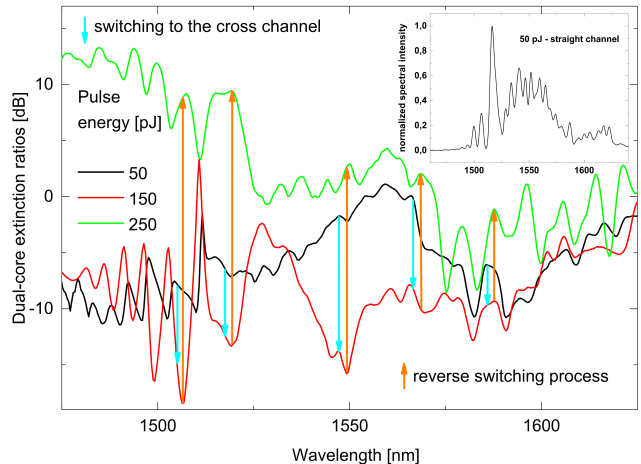


FIG. 4. The spectrally resolved extinction ratio between output intensities in the two channels, measured for different input energies, E . The inset displays the respective spectral intensity for $E = 50$ pJ.

[22], but achieved at lower pulse's energies. The switching performance includes forth and back switching steps, following the increase of the energy, at levels 100 – 150 pJ and 150 – 200 pJ, respectively. They correspond to the above-mentioned numerically predicted transitions from oscillations to the trapping in the cross channel, finally followed by the retention in the straight one.

The spectrally-resolved dual-core extinction ratio, $ER(\lambda)$, was calculated, on the basis of the experimental data, using power spectra $S_{\text{right}}(\lambda)$ and $S_{\text{left}}(\lambda)$, that were separately collected from both cores. The dependence of $ER(\lambda) \equiv 10 \lg(S_{\text{right}}(\lambda)/S_{\text{left}}(\lambda))$ on the input-pulse's energy, E , is showed in Fig. 4, revealing spectral details of the complex switching behavior, in correspondence with the camera images: at first, $ER(\lambda)$ decreases with the increase of E in the range of 50 – 150 pJ, then it increases between 150 and 250 pJ. The scenario of the all-optical soliton switching is supported by the fact that only moderate spectral broadening takes place and the switching is spectrally homogeneous. The same forth-and-back switching scenario, presented by the arrow pairs in Fig. 4, spanning in spectral range of 1510 – 1575 nm. This range covers the majority of the pulse energy taking into consideration the basic spectral profile presented in inset of Fig. 4. The forth switching step has lower contrast according to the spectral results comparing the length

of the cyan and orange arrows. The origin of this discrepancy is the chromatic aberration of the out-coupling optics avoiding the sharp separation of the two output spectra originating from the straight and cross channel [22]. Even though, the switching performance reveals clearly a possibility to direct the energy to either channel in a reversible way. An essential asset of the operation scheme produced in this work, in the theoretical and experimental form, is that it provides high switching contrasts without the requirement of precise adjustment of the fiber length.

As shown in Fig. 2, the simulations predict various possibilities to redirect the soliton between the two channels at $\eta = 0.78$, which corresponds to the pulse width in the experiment. Indeed, varying amplitude a at fixed $\eta = 0.78$, we cross several borders between regions corresponding to the self-trapping in the cross and straight channels. This complex structure exists due to the fact that, in the course of the self-compression, the initial pulse keeps oscillating between the channels, while the self-trapping occurs only if the soliton acquires a sufficiently high peak intensity. The pulsations persist in the course of several periods due to the interplay between the single-channel breathing of the deformed soliton and inter-core oscillations.

To summarize the comparison between the numerical and experimental results presented above, we note that the three values of the pulse's amplitude in Eq. (2), $a = 1.15$, 2, and 2.6, which give rise to the different outcomes of the transmission through the dual-core fiber, presented in Figs. 1 and 2 (quasi-linear oscillations, self-trapping in the cross channel, and retention in the straight one), correspond, in physical units, to incident-pulse energies 40, 120, and 205 pJ, respectively. The numerical results, obtained for this set of values of the energy, precisely correspond to the experimental results observed for energies 50, 150, and 250 pJ, which differ from their theoretical counterparts by a constant factor, ≈ 1.25 . Additional effects, such as third-order GVD and

Raman effects [1], account for the remaining discrepancy.

Losses may also affect the soliton propagation in the dual-core fiber. However, limited fiber lengths, for which the current experiments were performed, make dissipative effects a relatively weak perturbation, therefore they are not included in the theoretical model presented above.

In conclusion, reversible high-contrast switching performance of ultrafast quasi-solitons in the C-band is demonstrated in the strongly nonlinear dual-core fiber made of soft glass. Both experimental and numerical results reveal three different scenarios of the soliton propagation, *viz.*, periodic oscillations, self-trapping in the cross channel, and self-trapping in the straight one, depending on the energy of the incident pulse. The experimentally observed scenarios and transitions between them are predicted by systematic simulations of the system of coupled NLSEs. The results may be summarized as a well-defined forth-and-reverse soliton-switching effect, controlled by the monotonous increase of the pulse's energy. Such a sub-nanojoule high-contrast switching protocol may find applications to the design of all-optical signal-processing setups.

Funding This work is supported by the Polish National Science Center through project 2016/22/M/ST2/00261, IB and ML declare support from project No. 2016/23/P/ST7/02233 under POLONEZ program, which has received funding from the European Union's Horizon 2020 research and innovation program under the Marie Skłodowska-Curie grant agreement No 665778. B.A.M. acknowledges partial support from the Israel Science Foundation through grant No. 1286/17. N.V.H. was supported by Vietnam National Foundation for Science and Technology Development (NAFOSTED) under Grant Number 103.01-2017.55.

Disclosures The authors declare no conflicts of interest.

-
- [1] G. P. Agrawal, *Nonlinear Fiber Optics*, Academic Press: San Diego, CA, USA; ISBN 0-12-045143-3, (2001).
 - [2] S. M. Jensen, *IEEE J. Quantum Electron.* **18**, 1580 (1982).
 - [3] A. A. Maier, *Sov. J. Quantum Electron.* **12**, 1490 (1982).
 - [4] R. Hui, *Introduction to Fiber-Optic Communications*, Chap. 6 Academic Press, (2020).
 - [5] G. P. Agrawal, *Application of nonlinear fibre optics: 2nd edition*, Chap.2, Elsevier, (2008).
 - [6] S. R. Friberg, A. M. Weiner, Y. Silberberg, B. G. Sfez, and P. S. Smith, *Opt. Lett.* **13**, 904 (1988).
 - [7] G. I. Stegeman and A. Miller, *Photonics switching*, J. E. Midwinter, ed.(1993).
 - [8] S. Trillo, S. Wabnitz, E. M. Wright, and G. I. Stegeman, *Opt. Lett.* **13**, 672 (1988).
 - [9] M. Romagnoli, S. Trillo, and S. Wabnitz, *Opt. Quantum Electron.* **24**, 1237 (1992).
 - [10] Y. S. Kivshar, *Opt. Lett.* **18**, 79 (1993).
 - [11] P. L. Chu, Y. S. Kivshar, B. A. Malomed, G. D. Peng, and M. L. QuirogaTeixeiro, *J. Opt. Soc. Am. B* **12**, 898 (1995).
 - [12] K. S. Chiang, *Opt. Lett.* **20**, 997 (1995).
 - [13] I. M. Uzunov, R. Muschall, M. Goelles, Y. S. Kivshar, B. A. Malomed, and F. Lederer, *Phys. Rev. E* **51**, 2527 (1995).
 - [14] R. Driben and B. A. Malomed, *Opt. Lett.* **36**, 4323 (2011).
 - [15] A. Betlej, S. Suntsov, K. G. Makris, L. Jankovic, D. N. Christodoulides, G. I. Stegeman, J. Fini, R. T. Bise, and D. J. Digiovanni, *Opt. Lett.* **31**, 1480 (2006).
 - [16] P. Stajanca, D. Pysz, M. Michalka, G. Andriukaitis, T. Balciunas, G. Fan, A. Baltuska, and I. Bugar, *Laser Phys.* **24**, 065103 (2014).
 - [17] J. Herrmann, U. Griebner, N. Zhavoronkov, A. Husakou,

- A. D. Nickel, J. C. Knight, W. J. Wadsworth, P. S. Russell, and G. Korn, *Phys. Rev. Lett.* **88**, 1739011 (2002).
- [18] P. Stajanca and I. Bugar, *Laser Phys. Lett.* **13**, 116 (2016).
- [19] S. Minardi, F. Eilenberger, Y. V. Kartashov, A. Szameit, U. Ropke, J. Kobelke, K. Schuster, H. Bartelt, S. Nolte, L. Tomer, J. Lederer, A. Tiinnermann, and T. Pertsch, *Phys. Rev. Lett.* **105**, 263901 (2010).
- [20] M. Longobucco, J. Cimek, L. Curilla, D. Pysz, R. Buczynski, and I. Bugar, *Opt. Fiber Technol.* **51**, 48 (2019).
- [21] M. Longobucco, P. Stajanca, L. Curilla, R. Buczynski, and I. Bugar, *Laser Phys. Lett.* **17**, 025102 (2020).
- [22] L. Curilla, I. Astrauskas, A. Pugzlys, P. Stajanca, D. Pysz, F. Uherek, A. Baltuska, and I. Bugar, *Opt. Fiber Technol.* **42**, 39 (2018).
- [23] M. Longobucco, I. Astrauskas, A. Pugzlys, D. Pysz, F. Uherek, A. Baltuska, R. Buczynski, and I. Bugar, *Opt. Commun.* **472**, 126043 (2020).
- [24] M. Liu and K. S. Chiang, *Appl. Phys. B* **98** (2010).
- [25] J. Zhao, Z. Wang, Y. Liu, B. Liu, J. Zhao, Z. Wang, Y. Liu, and B. Liu, *Front. Optoelectronics China* **3**, 283 (2010).
- [26] J. H. Li, K. S. Chiang, and K. W. Chow, *Opt. Commun.* **318**, 11 (2014).
- [27] B. A. Malomed, *Solitons and nonlinear dynamics in dual-core optical fibers*, In: *Handbook of Optical Fibers*, Editor: G.-D. Peng, Springer, (2018).
- [28] J. Satsuma and N. Yajima, *Suppl. Prog. Theor. Phys.* **55**, 284 (1974).
- [29] J. Cimek, R. Buczynski, S. Couris, M. Klimczak, R. Stepien, and N. Liaros, *Opt. Mater. Express* **7**, 3471 (2017).